INFLUENCE OF LASER WAVELENGTH TO NANOPARTICLES GENERATION

Alexandru-Mihai IAMANDI[1,2]*, Liviu – Daniel GHICULESCU[3], Alexandru-DAN[5], Anca CRIVEANU[6], Nicu Doinel SCĂRIȘOREANU[4]

[1] Universitatea Națională de Știință și Tehnologie POLITEHNICA București, alexandru.iamandi@gmail.com
[2] Institutul Național pentru Fizica Laserilor, Plasmei și Radiației alexandru.iamandi@gmail.com
[3] Universitatea Națională de Știință și Tehnologie POLITEHNICA București, daniel.ghiculescu@gmail.com
[4] Institutul Național pentru Fizica Laserilor, Plasmei și Radiației, nicu.scarisoreanu@inflpr.ro
[5] Institutul Național pentru Fizica Laserilor, Plasmei și Radiației, alexandru.dan@inflpr.ro
[6] Institutul Național pentru Fizica Laserilor, Plasmei și Radiației, anca.criveanu@inflpr.ro

ABSTRACT: The influence of laser wavelength on laser ablation in liquids (LAL) is a critical factor in determining the efficiency, quality, and characteristics of nanoparticle generation. In LAL processes, varying the laser wavelength impacts the absorption efficiency of both the target material and the surrounding liquid, which in turn influences the thermal and mechanical effects responsible for nanoparticle formation [1]. Shorter wavelengths, often in the ultraviolet (UV) and visible range, generally lead to higher photon energy, enhancing photon absorption and improving ablation efficiency. This results in the generation of smaller, more homogeneous nanoparticles [2]. Conversely, longer wavelengths, such as those in the infrared (IR) range, are less absorbed by many materials and liquids, often producing larger particles with broader size distributions [3]. The selection of wavelength also affects secondary processes such as bubble formation, shockwave propagation, and plasma plume dynamics, which play significant roles in particle size, morphology, and composition [4]. Recent research has shown that tailoring the laser wavelength to the specific optical properties of the target and the medium allows for precise control over nanoparticle characteristics, which is crucial for applications in fields like biomedicine, catalysis, and electronics. This review summarizes the latest studies on the role of laser wavelength in LAL, highlighting the mechanisms of wavelength-specific interactions and their impact on nanoparticle properties [5].
.
KEYWORDS: nanoparticles, wavelength, liquid, LAL, infrared, ultraviolet

1. INTRODUCTION

The generation of nanoparticles via laser ablation in liquid (LAL) has emerged as a versatile and efficient method for producing nanomaterials with unique properties, critical for applications across fields such as catalysis, biomedical engineering, and electronics[1,4] This technique involves irradiating a solid target immersed in a liquid medium with a high-energy laser pulse, leading to rapid vaporization and ionization of the target material. The plasma plume generated by this interaction cools as it expands in the liquid, resulting in the nucleation and growth of nanoparticles. The ability to control particle size, shape, and stability by varying process parameters makes LAL highly adaptable and widely applicable in nanomaterial synthesis[3]

Among the factors affecting nanoparticle properties, the laser wavelength plays a particularly important role, as it directly influences the energy absorption of both the target material and the surrounding liquid. Shorter wavelengths, especially in the ultraviolet (UV) and visible ranges, are generally associated with higher photon energy, which enhances the laser energy absorption by the target and promotes efficient ablation. This often leads to smaller particle sizes with a more uniform size distribution due to more controlled nucleation processes in the plasma plume[2,3]. Conversely, longer wavelengths, such as those in the infrared (IR) range, typically result in less efficient energy absorption, often producing larger particles with a wider size distribution due to more turbulent plasma dynamics and less controlled particle formation [5].

Laser wavelength also influences secondary effects during LAL, such as cavitation bubble dynamics, shockwave formation, and plume expansion, all of which contribute to the stability and morphology of nanoparticles. For example, shorter wavelengths lead to more intense plasma formation, which impacts shockwave propagation and influences the cavitation bubble size, affecting nanoparticle aggregation and stability[1,4]. Research indicates that tailoring the laser wavelength to the optical properties of the target material and the liquid medium can therefore allow precise control over nanoparticle characteristics, which is crucial for optimizing performance in targeted applications[2,5]

This study investigates the influence of laser wavelength on the synthesis of nanoparticles via LAL, using various wavelengths to determine their effect on nanoparticle size, distribution, and stability. By examining laser wavelengths of 1064,

532, and 355 nm, this research aims to provide detailed insights into the impact of wavelength-specific mechanisms on nanoparticle formation, contributing to a deeper understanding of LAL as a controlled synthesis method for nanoparticle engineering.

This study outlines the principle of nanoparticle synthesis using a series of solid targets (Nickel, $Tb_xDy_{1-x}Fe_2$ with x = 0.6 and 0.7, TiO_2, Ag) and presents various experimental results obtained. For the experiments, wavelengths of 1064, 532, and 355nm were used, with a pulse frequency of 10 Hz and an ablation time of 20 minutes, corresponding to 12,000 pulses. As liquid suspensions, ultrapure water was used.

2. EXPERIMENTAL SETUP

The laser ablation process was conducted using a Pulsed Quantel QSMART 850 laser operating at its first harmonic wavelength of 1064 nm with Q-switching frequencies of 150, 100, and 50 microseconds. A Continuum laser was also employed to provide additional wavelengths of 532 nm, and 355 nm. The targets used were positioned within the reaction chamber, mounted on a holder located 2.5 cm above the base of the chamber. The laser beam, with an energy range of approximately 350–660 mJ, was directed onto the target surface through a series of mirrors aligned in the optical path.

To facilitate precise scanning, the reaction chamber (see figure 1) was mounted on a translation stage for X-axis movement, while Y-axis scanning was controlled using adjustable mounts. The target was submerged in ultrapure water (UPW) or in UPW containing 5 and 10 mM NaCl, depending on experimental requirements.

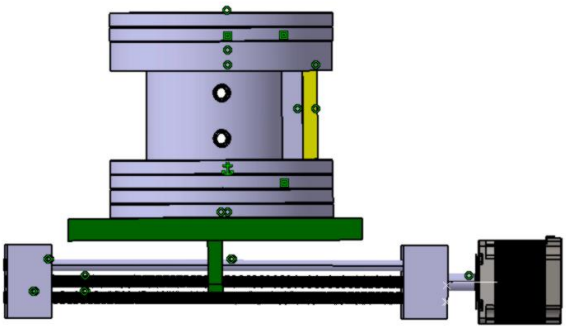

Figure 1. CAD model of laser ablation chamber

In the optical setup design (see Figure 2), considerations were given to the laser's positioning and the entrance aperture alignment for the laser beam in the ablation chamber. The laser beam was strategically directed to enter through the top of the chamber for optimal alignment.

Figure 3 illustrates the complete experimental setup, showing the ablation chamber fixed on the translation stage, allowing controlled X-axis movement of the laser beam. Y-axis control was achieved using a Kinesis K-Cube Brushed DC Servo Motor Controller by Thorlabs, a single-channel device designed for both manual and automated control of low-power (up to 15 V/2.5 W) brushed DC motors with encoder feedback.

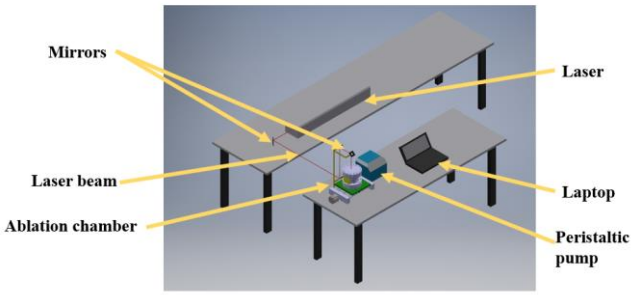

Figure 2. Isometric view of the designed setup

The mirrors used for guiding the laser beam and for Y-axis scanning were also manufactured by Thorlabs, designed to handle the fundamental, second, third, and fourth harmonic wavelengths of Nd

lasers. These mirrors are coated with dielectric layers, enabling high reflectance for both S and P polarizations and providing high damage resistance. The coatings are optimized for angles of incidence (AOI) between 0° and 45°, which allows for flexibility in optical configuration.

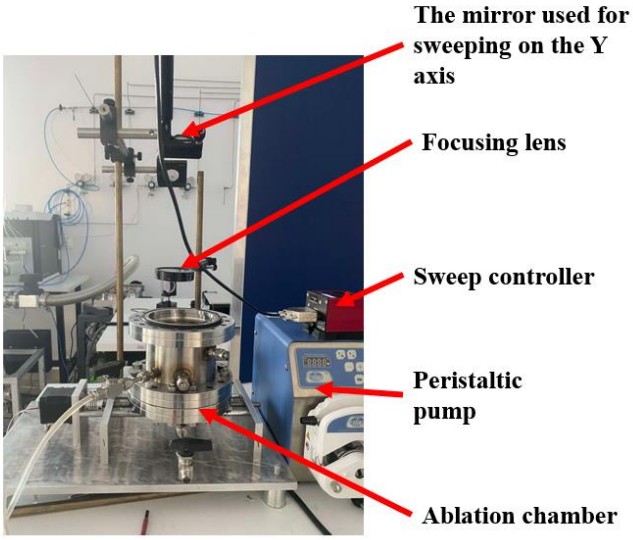

Figure 3. The experimental set

For implementing the X-axis targeting system of the liquid ablation chamber, electrical connections were configured according to the custom program

specified in the previous section and the TB6600 driver data sheet.

Pins 5, 2, and 8 on the Arduino development board were connected to the STEP, DIRECTION, and ENABLE pins of the TB6600 driver, respectively. The stepper motor wiring was completed in accordance with its datasheet, ensuring correct coil connections to the designated terminals on the TB6600 driver. Subsequently, the driver and Arduino Nano were connected to their respective power sources.

For the experiments, the TB6600 driver was configured with the following parameters:

- Microstepping setting: 2/8 microstepping
- Step resolution: 400 microsteps per revolution (switch configuration: off-on-on)
- Current limit: 2.8 A (switch configuration: off-off-off)

3. RESULTS AND DISCUSSION

The nanoparticles obtained from the liquid laser ablation process were subjected to characterization using various analytical techniques, including DLS (dynamic light scattering), AFM (atomic force microscopy), SEM (scanning electron microscopy) and EDX (X-ray energy dispersive spectroscopy). Following the characterization, a series of data were obtained, such as:

• Nanoparticle size

• Dispersion of nanoparticles in liquid suspension

• Type of nanoparticles

• Zeta potential

Zeta potential plays a fundamental role in evaluating the stability of nanoparticle dispersions, as it quantifies the electrostatic forces—either repulsive or attractive—that influence whether particles remain suspended or aggregate. Elevated absolute values of zeta potential (greater than ±30 mV) typically signify a stable dispersion, as strong electrostatic repulsion effectively prevents particle aggregation. Conversely, low absolute values of zeta potential (less than ±5 mV) are indicative of instability, where particles are prone to aggregation or sedimentation.

Based on data obtained from dynamic light scattering (DLS) analysis (presented in table 1), nickel nanoparticles synthesized via laser ablation in liquid demonstrate distinct stability characteristics depending on the laser wavelength used. For nanoparticles generated at a wavelength of 1064 nm, a positive zeta potential suggests a cationic surface charge, correlating with good stability in liquid dispersions over time. In contrast, samples prepared with a wavelength of 532 nm exhibit a anionic character and a corresponding reduction in stability, with the dispersions showing signs of instability. Nanoparticles produced at 355 nm consistently exhibit an cationic character and are characterized by a less stability in their liquid dispersions.

Table 1. Zeta potential of nanoparticles

Target material-laser wavelength	Zeta potential	DLS Size	Electrophoretic Mobility
Ni 1064nm	37.9 mV	365.9nm	0.000293 cm^2/Vs
Ni 532nm	-37.0 mV	203 nm	-0.000286 cm^2/Vs
Ni 355nm	10.6 mV	1410 nm	0.000081 cm^2/Vs
$Tb_xDy_{1-x}Fe_2$ 1064nm	43.8 mV	721 nm	0.000339 cm^2/Vs
$Tb_xDy_{1-x}Fe_2$ 532nm	42.1 mV	708 nm	0.000325 cm^2/Vs
$Tb_xDy_{1-x}Fe_2$ 355nm	45.6 mV	83 nm	0.000353 cm^2/Vs
TiO_2 532nm	-38.2 mV	238 nm	-0.000295 cm^2/Vs
TiO_2 355nm	-42.4 mV	9116 nm	-0.000328 cm^2/Vs
Ag 532nm	-54.4 mV	353 nm	-0.000420 cm2/Vs
Ag 355nm	-29.2 mV	739 nm	-0.000226 cm^2/Vs

As shown in Table 1, the nanoparticles synthesized using Terfenol (TbxDy1-xFe2) as a target exhibit a cationic character and high stability in the liquid suspension. This stability is further confirmed during a one-year observation period of the collected sample, as illustrated in Figure 4a. In contrast, nanoparticles produced from TiO_2 target display an anionic character and significantly lower stability over the same time interval, as depicted in Figure 4b. Silver nanoparticles are anionic (negatively charged), with a high magnitude of negative zeta potential indicating good dispersion stability.

Figure 4. a) $Tb_xDy_{1-x}Fe_2$ nanoparticles. b) TiO_2 nanoparticles

AFM (Atomic Force Microscopy) was performed to characterize (see figure 5,6) the nanoparticles that were obtained from laser ablation in liquid. The main image shows the topography of a nanoparticle sample. The color map (from dark orange to bright yellow/white) represents the height variations on the surface, where brighter areas are higher and correspond to nanoparticles, while darker areas represent the spaces between them. The scale bar on the left indicates height, in nanometres (nm), showing the vertical dimension of the nanoparticles on the substrate. The nanoparticles appear to be relatively uniform in size and densely packed across the surface.

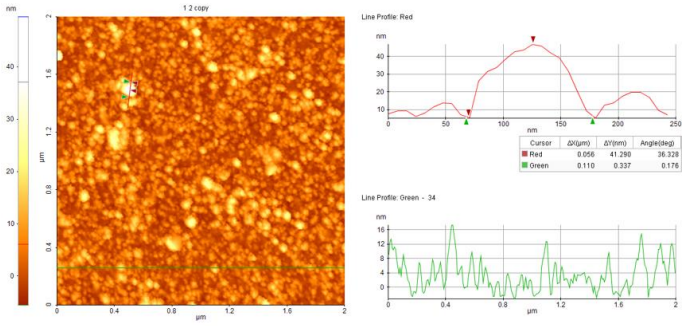

Figure 5. AFM characterization Ni nanoparticles, 1064nm, Qswitch 50, 300ml WPW

The top-right graph shows a line profile across the surface, highlighting the height variations of individual nanoparticles. Peaks in this graph correspond to individual nanoparticles or clusters, while valleys are the spaces between them.

The bottom-right graph shows a similar cross-sectional profile along a different axis or area of the surface. It also emphasizes the size distribution and spacing between nanoparticles.

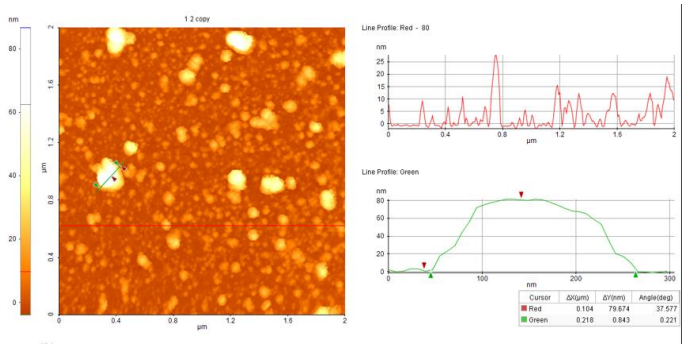

Figure 6. AFM characterization $Tb_xDy_{1-x}Fe_2$ nanoparticles, 1064nm, Qswitch 50, 300ml WPW

The histogram provides a distribution of nanoparticle heights. The X-axis represents the height (in nm), and the Y-axis shows the frequency of those heights. A narrow peak in the histogram would suggest uniform nanoparticle size, while a broader peak would indicate a wider size distribution. The particles likely have a range of heights, with most heights clustered around the peak of the histogram.

Nickel nanoparticles are smaller and more uniform, with heights mostly under 20 nm. Terfenol nanoparticles are larger and more irregular, with some reaching ~80 nm. Nickel nanoparticles exhibit lower roughness (Rq≈4.4 nm). Terfenol nanoparticles have much higher roughness (Rq≈31.5 nm) due to their larger size and irregular distribution.

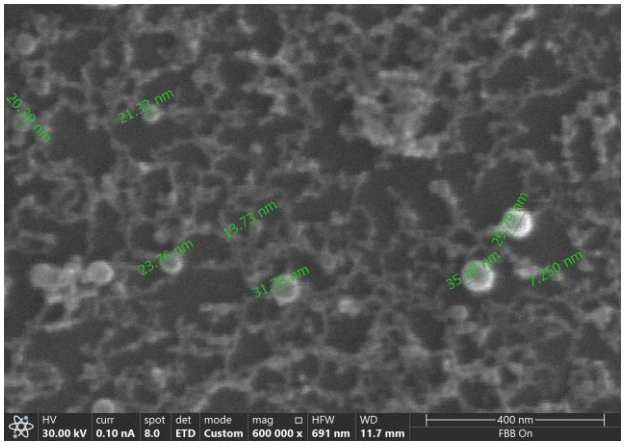

Figure 7. SEM characterization $Tb_xDy_{1-x}Fe_2$ nanoparticles, 1064nm, 300ml WPW

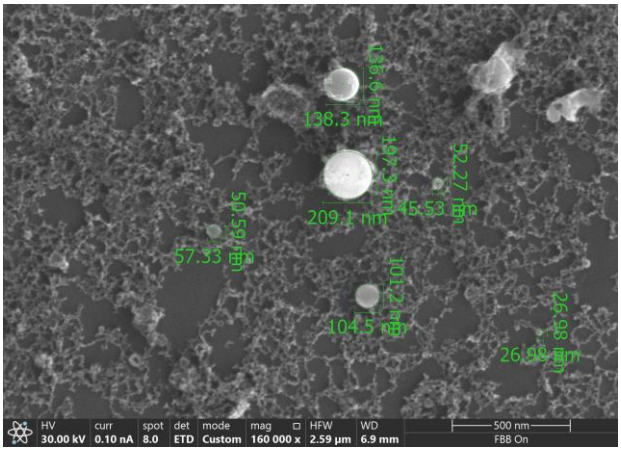

Figure 8. SEM characterization $Tb_xDy_{1-x}Fe_2$ nanoparticles, 532nm, 300ml WPW

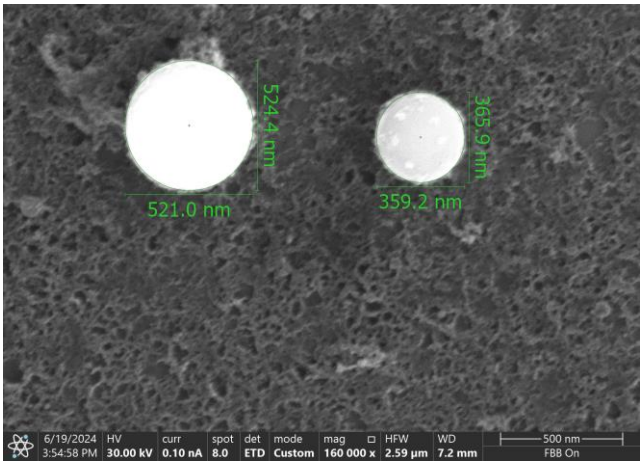

Figure 9. SEM characterization $Tb_xDy_{1-x}Fe_2$ nanoparticles, 355nm, 300ml WPW

The three images above illustrate the SEM views of terfenol nanoparticles produced by laser ablation in liquid using three different laser wavelengths: 1064 nm (infrared), 532 nm (green), and 355 nm (ultraviolet).

In figure 7, it is presented smallest nanoparticles among the three wavelengths. The particles appear highly dispersed, with minimal evidence of agglomeration. While infrared wavelengths generally result in larger particles due to lower photon energy, specific experimental factors such as laser fluence, pulse duration, target material properties, and liquid environment could lead to unexpected size outcomes.

For instance, efficient thermal ablation coupled with controlled cooling could produce smaller particles in this case. Additionally, higher wavelengths may avoid excessive plasma shielding, allowing more consistent ablation of the target material. Studies such as those by Zeng et al. (2007) emphasize that other experimental parameters can sometimes override the general wavelength trends in particle size[6].

In the experiment were 532nm laser wavelength was used (figure 8), nanoparticles are slightly larger and less uniform compared to those produced at 1064 nm. Some evidence of aggregation is present. The green wavelength provides intermediate photon energy, often leading to effective material ablation. However, the particle size in this case might reflect less efficient cooling or plasma confinement compared to 1064 nm. Plasma dynamics at this wavelength can lead to higher particle growth rates, as described by Amendola & Meneghetti (2009) [8].

In the experiment were 355nm laser wavelength was used (figure 9), nanoparticles appear larger and more irregular compared to those at 1064 nm and agglomeration is more noticeable. Despite the higher photon energy of UV light, this result could be due to excessive plasma shielding, which inhibits consistent energy delivery to the target material.

Additionally, rapid quenching can sometimes lead to larger, irregular fragments instead of uniformly smaller particles, as noted in studies by Fazio et al. (2015). Experimental setup or energy fluence might have further influenced the unexpected size increase[8].

The images corresponding to laser ablation in liquid at three different wavelengths (1064 nm, 532 nm, and 355 nm) of silver target are displayed below.

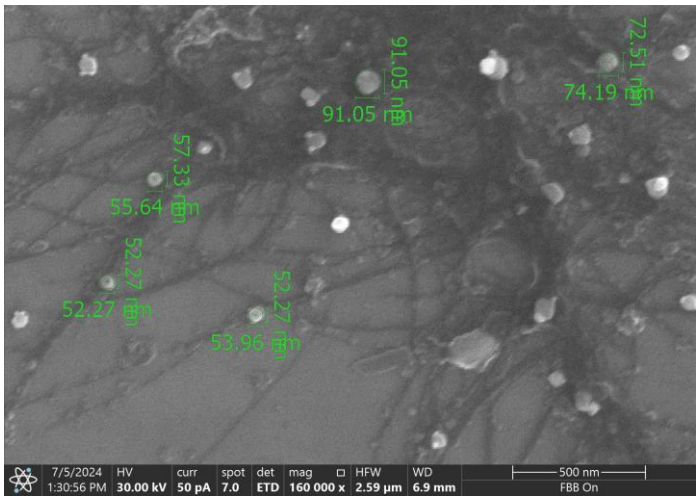

Figure 10. SEM characterization silver nanoparticles, 1064nm, 300ml WPW

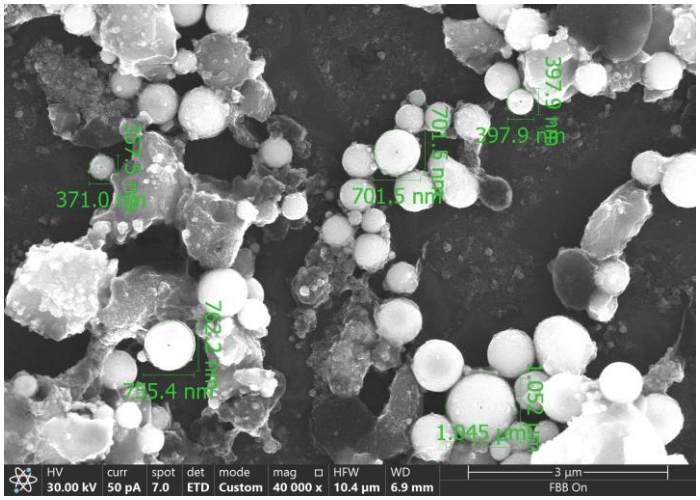

Figure 11. SEM characterization silver nanoparticles, 532nm, 300ml WPW

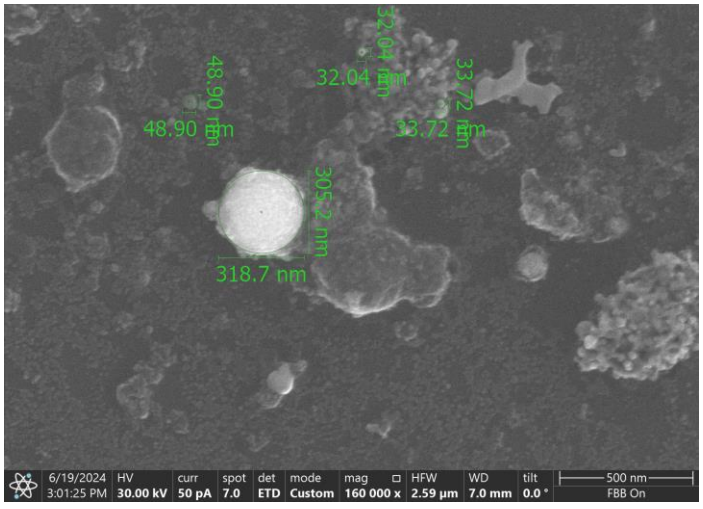

Figure 12. SEM characterization silver nanoparticles, 355nm, 300ml WPW

In first image, (Figure 10) using 1064 nm wavelength it produces the smallest particles due to efficient fragmentation during laser ablation in liquids. Studies [9,10] indicate that longer wavelengths like 1064 nm deposit energy over a broader area, leading to fine and dispersed particles.

In experiment were 532nm wavelength was used, from SEM characterisation we have the highest average particle size among the three wavelengths can be attributed to localized heating and melting caused by the moderate photon energy at this wavelength [11]. This leads to aggregation, reducing the density of distinct nanoparticles.

Such behavior is well-documented for green lasers, where energy absorption and material melting dominate nanoparticle morphology [7].

Studies indicates that short wavelengths like 355 nm offer high photon energy, leading to rapid ablation and localized melting, which supports the formation of intermediate particle sizes [12], as it cand pe observed in figure 12. These shorter wavelengths can also cause partial aggregation, as observed in experimental studies of UV laser ablation [13].

The images corresponding to laser ablation in liquid at three different wavelengths (1064 nm, 532 nm, and 355 nm) of TiO_2 target are displayed below.

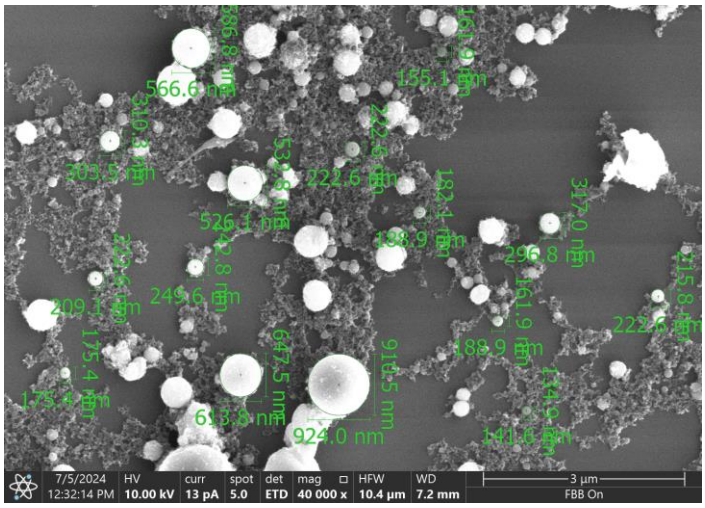

Figure 13. SEM characterization TiO_2 nanoparticles, 1064nm, 300ml WPW

Using 1064nm wavelenght fot laser ablation proces of TiO_2 target results in a broad distribution of particle sizes, with the largest maximum diameter. The high variability suggests uneven energy deposition, leading to a mix of smaller and larger particles.

At 532nm wavelengt, despite the mean size is smaller than at 1064 nm, the distribution is also quite broad, showing a mixture of very small and some exceptionally large particles. The green wavelength typically has better material absorption, but some clustering may occur.

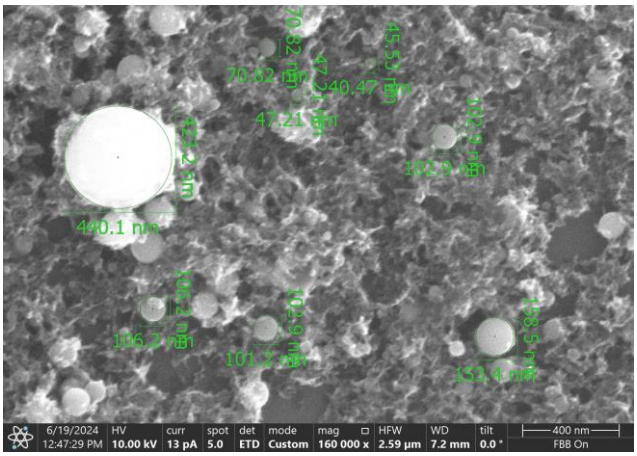

Figure 14. SEM characterization TiO_2 nanoparticles, 532nm, 300ml WPW

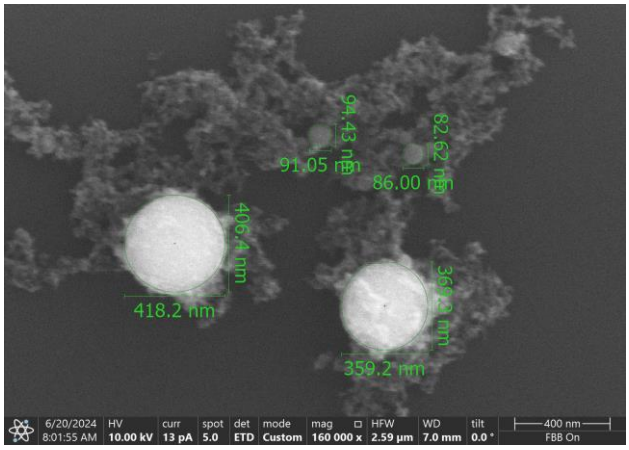

Figure 15. SEM characterization TiO_2 nanoparticles, 355nm, 300ml WPW

UV light produces particles with a tighter size range, though some variability is still evident. The higher energy of this wavelength likely enhances the ablation efficiency, producing smaller and more consistent particles compared to 1064 nm.

4. CONCLUSION

From AFM characterisation we observe that nickel nanoparticles exhibit uniform size and smooth distribution, with heights predominantly below 20 nm. Terfenol nanoparticles show larger particle size and greater height variations, with some particles reaching up to 80 nm. Based on the dynamic light scattering (DLS) data presented in the table 1, the observed large nanoparticle size can be attributed to the absence of a surfactant, which would otherwise facilitate their dispersion within the suspension.

From SEM characterization of terfenol nanoparticles contrary to conventional expectations, the smallest and most uniform nanoparticles were observed at 1064 nm (infrared). This suggests that specific experimental conditions, such as controlled ablation and effective thermal quenching, played a significant role in particle size minimization at this wavelength.

Using 532 nm (green) produced slightly larger, less uniform particles, likely due to plasma dynamics that promoted some agglomeration during the cooling phase.

Using 355 nm (ultraviolet) resulted in the largest and most irregular nanoparticles, possibly due to excessive plasma shielding and rapid quenching, which disrupted uniform particle formation.

Laser wavelength significantly influences nanoparticle size and density during ablation. Longer wavelengths (1064 nm) produce higher-density nanoparticles with smaller dimensions, ideal for applications requiring uniform nanoscale particles. In contrast, shorter wavelengths (532 nm and 355 nm) generate larger particles with lower densities due to higher photon energy promoting aggregation and coalescence.

The choice of laser wavelength determines nanoparticle properties tailored to specific applications. The 1064 nm wavelength is optimal for high-density, fine nanoparticles suitable for catalysis and biomedical uses. Meanwhile, 532 nm and 355 nm wavelengths are more appropriate for optical or plasmonic applications, where larger particle sizes enhance performance through strong light-matter interactions.

From SEM images of TiO_2 nanoparticles it can be observed that using 1064 nm wavelength produces relatively larger nanoparticles on average. Using 532nm wavelength produces smaller nanoparticles on average compared to 1064 nm, but it exhibits a higher variability in size and using 355nm wavelength produces the smallest particles, with a narrower size distribution compared to the other wavelengths.

5. ACKNOWLEDGEMENTS

It is stated that these applied contributions would not have been possible without the access to the available technical and material resources, to the equipment provided by the National Institute for the Physics of Lasers, Plasma and Radiation (INFLPR) and the expertise accumulated in this advanced field within the institute. Liquid laser ablation experiments were carried out at the Photonics and Plasma Innovation Center for Advanced Materials and Technologies (Photoplasmat C400).

6. REFERENCES

1. Zeng, H., Du, X.-W., Singh, S. C., et al. Nanomaterials via laser ablation in liquid: A review. Advanced Functional Materials, 22(6), 1333-1353, (2012).
2. Tsuji, T., Yoon, S.-H., Tsuji, M., et al. Effects of laser wavelength on size distributions of colloidal silver nanoparticles prepared by laser ablation in aqueous solutions. Applied Surface Science, 254(16), 5224-5230, (2007).
3. Semaltianos, N. G. (2010). Nanoparticles by laser ablation. Critical Reviews in Solid State and Materials Sciences, 35(2), 105-124.
4. Barcikowski, S., Menéndez-Manjón, A., Chichkov, B., & Hartmann, T. Laser ablation in liquids: A powerful tool for producing nanoparticles. Journal of Laser Applications, 21(2), 83-93, (2009).
5. Yang, G. W. Laser ablation in liquids: Applications in the synthesis of nanocrystals. Progress in Materials Science, 52(4), 648-698, (2007).
6. Zeng, H., Cai, W., Liu, P., Xu, X., & Yang, G. W. (2007). Nanomaterials via laser ablation/irradiation in liquid: A review. *Applied Surface Science*, 253(17), 6872-6880.
7. Amendola, V., & Meneghetti, M. (2009). Laser ablation synthesis in solution and size manipulation of noble metal nanoparticles. *Physical Chemistry Chemical Physics*, 11(20), 3805-3821.
8. Fazio, E., Gökce, B., & Amendola, V. (2015). Nanoparticles engineering by pulsed laser ablation in liquids: Concepts and applications. *Optik - International Journal for Light and Electron Optics*, 127(15), 7096-7101.
9. Zeng, H., et al. (2013). "Nanomaterials via Laser Ablation in Liquids: A Review." *Advanced Functional Materials*, 24(5), 693–710.
10. Sylvestre, J.-P., et al. (2004). "Synthesis and Stabilization of Silver Nanoparticles via Laser Ablation in Liquids." *Journal of the American Chemical Society*, 126(23), 7176–7177.
11. Tsuji, T., et al. (2008). "Laser-Induced Nanoparticle Formation in Liquids for Metal and Metal Oxide Systems." *Applied Surface Science*, 254(16), 5224–5230.
12. Kumar, V., et al. (2010). "Laser Ablation in Liquid: A Novel Method for Nanomaterials Synthesis." *Current Science*
13. Bulgakov, A. V., & Ozerov, I. (2010). "Laser-Induced Nanoparticle Formation via Ablation in Liquids." *Chemical Physics Letters*, 487(4–6), 274–278.